Using response surface methodology to evaluate electrocoagulation in the pretreatment of produced water from polymer-flooding well of Dagang Oilfield with bipolar aluminum electrodes

Mi-jia Zhu[a], Jun Yao[a,b,*], Wen-bin Wang[c], Xian-qing Yin[c], Wu Chen[c], Xiao-ying Wu[a]

[a]*School of Civil and Environmental Engineering, National "International Cooperation Based on Environment and Energy", University of Science and Technology Beijing, 100083 Beijing, P.R. China, Tel./Fax: +86 10 62333305; emails: zhumijia128@163.com (M.-j. Zhu), yaojun@ustb.edu.cn (J. Yao), wxy-0703@qq.com (X.-y. Wu)*
[b]*State Key Laboratory of Biogeology and Environmental Geology and Sino-Hungarian Joint Laboratory of Environmental Science and Health, University of Geosciences, 430074 Wuhan, P.R. China*
[c]*Key Laboratory of Exploration Technologies for Oil and Gas Resources, Yangtze University, 434000 Jingzhou, P.R. China, Tel. +86 716 8060472; email: wwb_306@163.com (W.-b. Wang), jzyinxq@126.com (X.-q. Yin), ccww98@126.com (W. Chen)*

ABSTRACT

The wide use of polymers to enhance oil recovery can make pumping and rejecting oilfield produced water difficult because of the high viscosity of the treated water. To deal with this problem, this study proposed an electrocoagulation method that is time saving, highly efficient, and easy to apply. A Box–Behnken design coupled with the response surface methodology (RSM) was used to construct a model of the electrocoagulation process that considers three key variables: current density, inter-electrode gap, and operation time. The optimized operational conditions were obtained using second-order polynomial models; they were a current density of 45.6 mA/cm^2, an inter-electrode of 3.2 cm, and an operation time of 22.8 min. The results under these conditions were a viscosity reduction of 90.9% and a chemical oxygen demand (COD) reduction of 74.9%. These data strongly correlated with the predicted values of the RSM models. Based on the single and interactive effect analysis, it showed that viscosity and COD reduction efficiency enhanced with increasing operation time. The efficiencies were increased when current density was raised from 20 to 40 mA/cm^2 and subsequently decreased from 40 to 60 mA/cm^2. They were also increased while inter-electrode gap was enlarged from 2.0 to 4.0 cm and then decreased from 4.0 to 6.0 cm. Furthermore, the practicability of the polymer-flooding produced water treatment under the optimized conditions was proved by UV–vis, zeta potential, and particle size measurement.

Keywords: Polymer-flooding produced water; Electrocoagulation; Response surface methodology; Viscosity reduction; COD reduction

*Corresponding author.

1. Introduction

Polymer flooding is an enhanced oil recovery method that can efficiently recover remaining oil by injecting water with a polymer (polyacrylamide) to increase its viscosity during the displacing phase. It can enhance crude oil recovery by up to 12% and plays a vital role in oil production [1–4]. However, with the development of the mechanical processing industry, the amount of oily polymer-flooding produced water (OPFPW) has increased. This water has deleterious effects on the operation of wastewater treatment due to its high viscosity, which reduces the efficiency of pumping and rejecting, and can even destroy pumps.

Previous studies have developed several techniques for treating this type of wastewater, including chemical methods [5–8], physical separation [9–11], biological degradation [12–14], and combined methods [15–18]. However, some of these processes are complex, require specialized manpower, and are time consuming. In this study, the electrocoagulation method was proposed and tested as an OPFPW treatment. This method is not only fast and requires only simple equipment, but is very versatile and has been used to treat a wide range of industrial effluents [19,20]. The process does not use chemicals; instead, consumable metal plates (such as aluminum and iron) are used as sacrificial electrodes that continuously produce ions in the system. Due to the high adsorption and coagulation efficiency of Al^{3+} ions, aluminum plates were used as electrode materials in this experiment [21,22]. In the electrocoagulation process, the released cations neutralize the charges of the headgroups of the polymer molecules and thereby initiate coagulation. The formed flocs are separated from the aqueous phase by sedimentation or flotation [23,24]. The electrochemical reactions occurring at the anode are shown below in Eqs. (1)–(4):

$$Al_{(s)} \rightarrow Al^{3+}_{(aq)} + 3e^- \tag{1}$$

$$2H_2O_{(l)} \rightarrow O_{2(g)} + 4H^+_{(aq)} + 4e^- \tag{2}$$

$$Al^{3+}_{(aq)} + 3H_2O_{(l)} \rightarrow Al(OH)_{3(aq)} + 3H^+_{(aq)} \tag{3}$$

$$nAl(OH)_{3(aq)} \rightarrow Al_n(OH)_{3n(aq)} \tag{4}$$
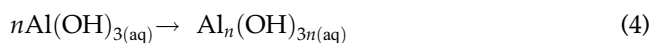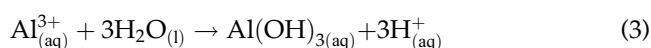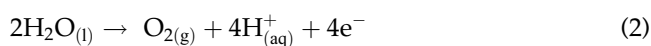
The reaction at the cathode is written as follows:

$$2H_2O_{(l)} + 2e^- \rightarrow H_{2(g)} + 2OH^-_{(aq)} \tag{5}$$

Moreover, a large number of chloride ions in the produced water scavenge oxygen to form hypochlorite (ClO^-) at the electrode, and ClO^- ions act as an oxidizing agent that favors the electrochemical reaction [25]. The following reactions explain the formation of ClO^- ions:

$$2Cl^-_{(aq)} \rightarrow Cl_{2(g)} + 2e^- \tag{6}$$

$$Cl_{2(g)} + H_2O_{(l)} \rightarrow HClO_{(aq)} + H^+_{(aq)} + Cl^-_{(aq)} \tag{7}$$

$$HClO_{(aq)} \rightarrow ClO^-_{(aq)} + H^+_{(aq)} \tag{8}$$
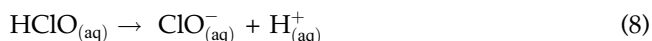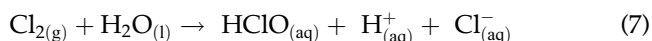
Previous experimental investigations have examined the effects of different operational parameters, such as initial pH, salt concentration, temperature, electric current density, inter-electrode distance, and operation time, on the electrocoagulation efficiency [20,26–28]. The one-factor-at-a-time approach has been used to study the effects of various factors on the treatment; however, this conventional method is time consuming for multi-variable systems and fails to estimate the interactive effects among factors [29]. The response surface methodology (RSM), which generates a mathematical model, is an alternative method for defining the effect of all of the independent variables, alone or in combination [30–32].

The objectives of this study were to investigate the individual and combined effects of current density, inter-electrode gap, and operation time on polymer solution treatment, and to optimize the process variables for the maximum reduction of the chemical oxygen demand (COD) and viscosity using a Box–Behnken response surface design. The results will be helpful to the design of an EC unit for the pretreatment of OPFPW.

2. Materials and methods

2.1. Preparation of the electrolyte solution

Formation water was collected from the Gangxi 43# oil well. The pH value and ionic composition were measured using a HQ11D pH meter (Hach Co., Ltd, USA) and an ionic meter (Hangchuang Co., Ltd, Shenzhen, Guangdong, China), respectively. To simulate the formation water, potassium chloride, sodium chloride, and other metal salts were added to distilled water at the dosages as shown in Table 1. The initial pH value of the solution was adjusted with sodium hydroxide and sulfuric acid solution. All of the chemicals and reagents used were of analytical grade. A

polyacrylamide solution of 300 ppm was prepared by dissolving 0.30 g of polyacrylamide (AP-P4, collected from Dagang Oilfield Company; the average molecular weight is 12 million, the solubility in water is 27%) into 1,000 mL water. The structural formula of AP-P4 can be seen in Fig. 1. To avoid the interference effect of the oil on the COD and viscosity detection, the laboratory prepared polymer-flooding water (LPPFW, without add crude oil) was used in a series of batch experiments with Box–Behnken design.

2.2. Electrolytic cell

The lab-scale reactor is shown in Fig. 2. Electrocoagulation experiments were carried out in a cylindrical glass ($\Phi = 17.5$ cm, $h = 12$ cm^2). In this process, aluminum plates (purity, $\geq 98\%$; thickness, 0.2 cm; size, 10 cm × 10 cm) were 0.2 cm thick with the dimensions 10 cm × 10 cm were used as electrodes. One-half of the electrodes were immersed in the electrolyte solution, making the effective surface area of the electrode 50 cm^2. The electrolysis solution to be treated with a volume of 1,000 mL was poured into a magnetically stirred tank. Agitation at 200 rpm was provided by means of a magnetic stirrer. A power source (WKY-505, East Co., Ltd, Huizhou, Guangdong, China) was used to provide current density to the EC cell. The electrodes were connected to a digital DC supply characterized by current range (0–5 A) and volt range (0–50 V). All of the experiments were conducted at room temperature (28°C). At the end of the experiments, samples were filtered to remove any sludge and analyzed for viscosity and COD reduction.

2.3. Detection methods

To monitor the electrocoagulation, the viscosity of the water samples was measured using a viscometer with an LV-1 rotor with a speed of 100 rpm at 55 °C. The COD of the samples was measured with a QCOD-2E rapid determination meter (Changhong Co., Ltd, Shenzhen, Guangdong, China). The COD of the
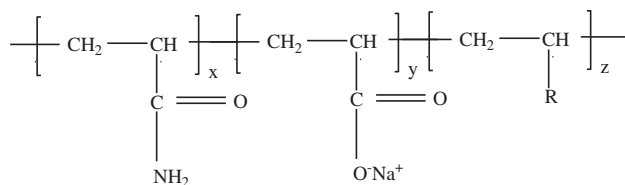
Fig. 1. Structural formula of AP-P4. R: hydrophobic side group, carbon number: 16–20.

samples was quantified using the standard methods for the examination of water and wastewater (Washington, DC, USA, 1998). The ultraviolet spectrum of the samples was detected using a UV-1,800 UV-vis spectrophotometer (Shimadzu Co., Ltd, Kyoto, Japan). Observations of floc formation in the electrocoagulation process were carried out after the suspension stand for 20 min. The pH value of the electrolyte was measured by PHS-25 pH meter (Yidian Co., Ltd, Shanghai, China). The sizes and zeta potentials of the suspensions were detected using a nanozetasizer (Malven Co., Ltd, UK).

2.4. Determination of the range of process variables

A preliminary study was carried out to narrow the range of parameters for optimization. In the preliminary experiments, a current density range of 20–100 mA/cm^2, an inter-electrode gap range of 2–8 cm, and an operation time range of 5–40 min were examined. Based on the preliminary results, the study ranges chosen for the current density, inter-electrode gap, and operation time in the final experiment were 20–60 mA/cm^2, 2–6 cm, and 15–25 min, respectively.

2.5. Experimental design

The RSM was used for the experimental design, data analysis, and model construction. The aim was to investigate the relationship between viscosity, COD reduction efficiency, and three operating parameters (i.e. current density, inter-electrode gap, and operation

Table 1
Preparation of laboratory simulated formation water in Gangxi 43# well

Parameter	Concentration (mg/L)	Parameter	Concentration (mg/L)
pH	8.28	Na$_2$SO$_4$	37.26
KCl	25.94	NaHCO$_3$	1,100.04
NaCl	6,679.71	Na$_2$CO$_3$	71.78
CaCl$_2$	334.30	AP-P4 (polyacrylamide)	300.00
MgCl$_2$	216.44		
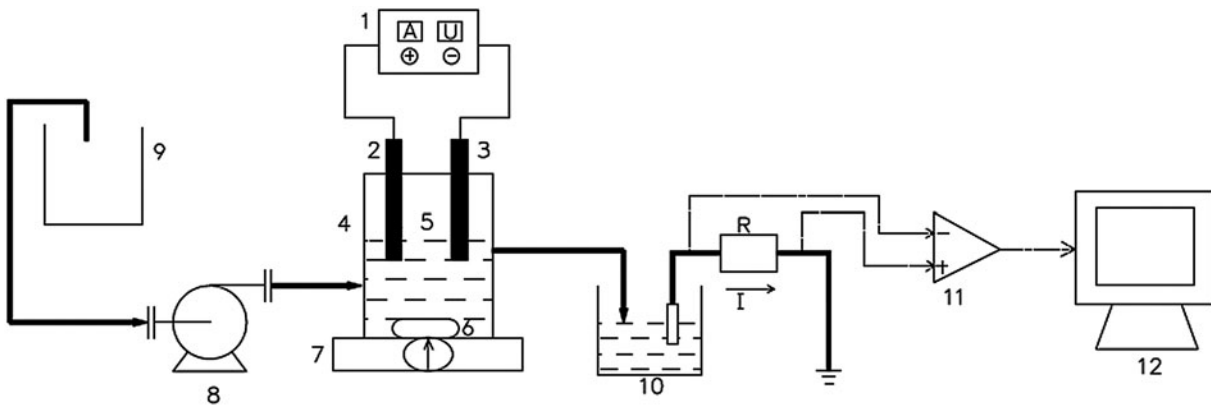
Fig. 2. Electrocoagulation equipment.
Notes: (1) power source, (2) parallel anode, (3) parallel cathode, (4) electrocoagulation cell, (5) electrolysis solution, (6) magnetic bar stirrer, (7) magnetic stirrer, (8) pump, (9) produced water tank, (10) treated water collector, (11) nanozetasizer, and (12) computer.
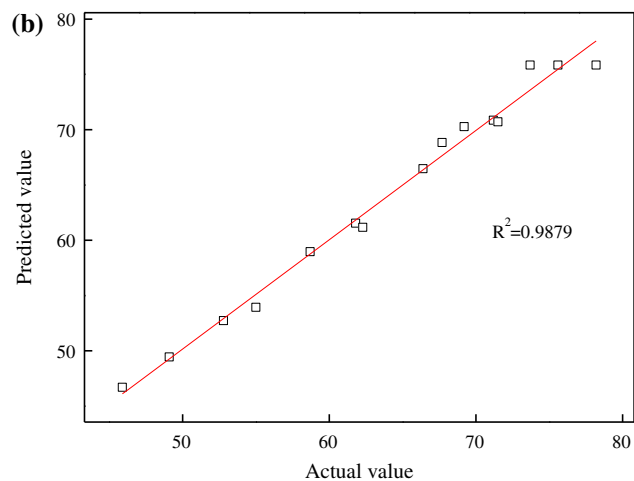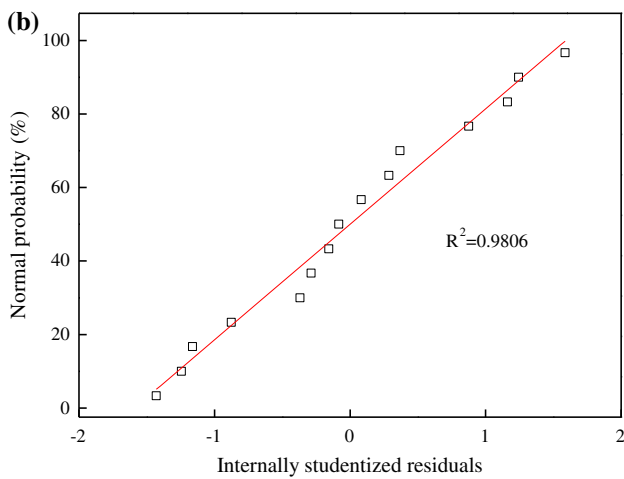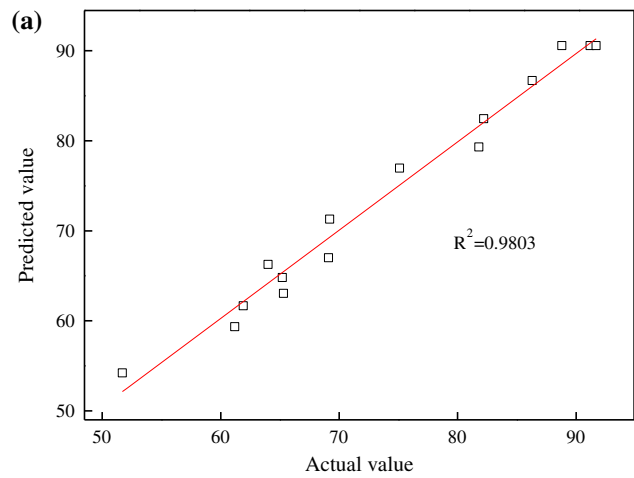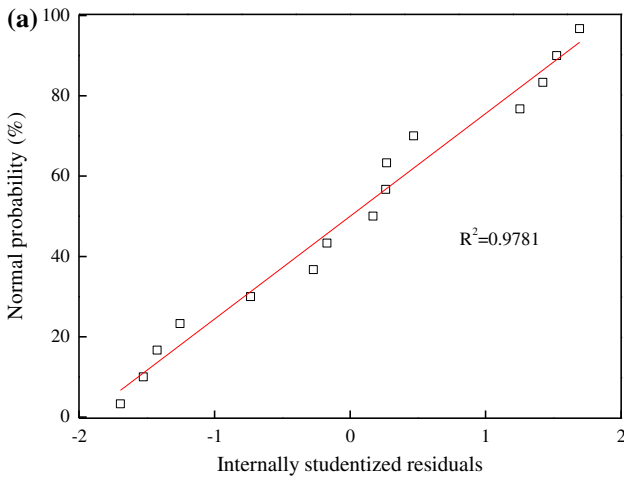
Fig. 3. Normal probability plot of the internally studentized residuals in the model of (a) viscosity reduction and (b) COD reduction efficiency based on Box–Behnken design.

Fig. 4. Predicted vs. actual values plot for (a) viscosity reduction and (b) COD reduction efficiency in response surface model (linear fitting plot).

Table 2
Experimental range and levels of the independent variables (current density, inter-electrode gap, operation time) in Box–Behnken design

Variables, unit	Factors	Ranges and levels		
		−1	0	1
Current density (mA/cm^2)	X_1	20	40	60
Inter-electrode gap (cm)	X_2	2.0	4.0	6.0
Operation time (min)	X_3	15	20	25

time). The Box–Behnken design (BBD) was specifically selected as it was more efficient than other RSM designs when there are three or four variables [29,33]. Table 2 shows the Box–Behnken design matrix. The three selected process variables, current density, inter-electrode gap, and operation time, were defined as X_1, X_2, and X_3, respectively. Each parameter was coded at three levels, −1 (minimum), 0 (central), and +1 (maximum), covering the entire study range. The two responses, viscosity reduction and COD reduction efficiency, were defined as Y_1 and Y_2, respectively.

2.6. Statistical analysis

Analysis of variance (ANOVA) was used to analyze the experimental data. The adequacy of the developed models was measured by coefficient of determination (R^2) and adjusted coefficient of determination (R^2_{adj}) analyses. After fitting the models, the generated data were used for 3D response surface optimization. All of the statistical analyses were conducted using Design Expert 8.0 software (Stat Ease Inc., Minneapolis, USA).

2.7. Calculation of operating costs

In the electrocoagulation process, the operating costs contain consumption of electrical energy, electrode materials (especially sacrificial electrode), cost of sludge disposal, etc. [34]. In this preliminary economic calculation, electrical energy and electrode costs were taken into account as major items and the operating cost equation was described as follows:

$$\text{Operating cost} = aC_{\text{energy}} + bC_{\text{electrodes}} \quad (9)$$

where C_{energy} (kW h/m^3) and $C_{\text{electrodes}}$ (kg Al/m^3) are consumption quantities for treatment of produced water, a and b coefficient for Chinese market in 2014 are as follows:

(1) Coefficient a: industrial electrical energy price = 0.1167$/kW h;
(2) Coefficient b: wholesale electrode material price = 2.1498$/kg Al.

3. Results and discussion

3.1. Box–Behnken design

A Box–Behnken design requires an experiment number according to $N = k^2 + k + C_p$, where k is the factor number and C_p is the replicate number of the central point. Experimental data from the Box–Behnken design can be analyzed and fitted to a second-order model using Design Expert 8.0 software and the following equation:

$$Y = \beta_0 + \sum_{i=1}^{k} \beta_i X_i + \sum_{i=1}^{j-1} \sum_{j=1}^{k} \beta_{ij} X_i X_j + \sum_{i=1}^{k} \beta_{ii} X_i^2 + e_i \quad (10)$$

where Y is the response for viscosity reduction efficiency (Y_1) or COD reduction efficiency (Y_2), β_0 is a constant coefficient, X_i and X_j are variables, β_i is a coefficient that determines the influence of parameter i in the response (linear term), β_{ij} refers to the effect of the interaction among variables i and j, β_{ii} is a parameter that determines the shape of the curve, k is the number of studied factors, and e_i is the error. The coded values of the process parameters in Eq. (10) can be determined by the following equation:

$$X_i = \frac{x_i - x_0}{\Delta x_i} \quad (11)$$

In Eq. (11), X_i is the dimensionless coded value of the ith independent variable, x_i is the uncoded value of the ith independent variable, x_0 is the uncoded ith independent variable at the center point, and Δx_i is the step change value between the low level (−1) and high level (+1) [35]. The low, middle, and high levels of each variable are illustrated in Table 2.

3.2. ANOVA and model fitting

Table 3 shows the experimental results for the viscosity and COD reduction efficiencies based on the Box–Behnken design. The results of the ANOVA of the regression parameters of the predicted response surface quadratic models for viscosity and COD reduction efficiency, with insignificant model terms excluded, are shown in Tables 4 and 5, respectively. The relationships between viscosity, COD reduction

Table 3
Design matrix in coded units and the experimental responses

Run number	Current density (X_1)	Inter-electrode gap (X_2)	Operation time (X_3)	Viscosity reduction efficiency (Y_1, %)	COD reduction efficiency (Y_2, %)
1	−1	1	0	69.1	58.7
2	−1	−1	0	65.3	62.3
3	0	−1	1	86.3	69.2
4	1	0	−1	61.2	52.8
5	1	0	1	81.8	71.5
6	1	1	0	64.0	67.7
7	0	0	0	91.2	78.2
8	−1	0	1	75.1	66.4
9	0	0	0	88.8	73.7
10	−1	0	−1	51.7	45.9
11	0	1	−1	65.2	55.0
12	0	−1	−1	61.9	49.1
13	0	0	0	91.7	75.6
14	0	1	1	82.2	71.2
15	1	−1	0	69.2	61.8

efficiency, and the three operating parameters (i.e. current density, inter-electrode gap, and operation time) were fitted to the second-order polynomial Eqs. (12) and (13) as given below:

$$Y_1 = 90.57 + 1.87X_1 - 0.28X_2 + 10.68X_3 - 2.25X_1X_2 \\ - 0.7X_1X_3 - 1.85X_2X_3 - 15.06X_1^2 - 8.61X_2^2 \\ - 8.06X_3^2 \tag{12}$$

$$Y_2 = 75.83 + 2.56X_1 + 1.27X_2 + 9.44X_3 + 2.38X_1X_2 \\ - 0.45X_1X_3 - 0.98X_2X_3 - 7.59X_1^2 - 5.62X_2^2 \\ - 9.09X_3^2 \tag{13}$$

where Y_1 and Y_2 denote, respectively, the viscosity reduction rate (%) and COD reduction rate (%); X_1, X_2, and X_3 denote the coded values for current density (mA/cm^2), inter-electrode gap (cm), and reaction time (min), respectively.

For the viscosity reduction efficiency, the F-value of 27.70 implied that the model was significant. The p-values less than 0.05 indicated that the model terms X_3, X_1^2, X_2^2, and X_3^2 were significant, as described in Table 4. Moreover, the lack-of-fit value of 5.37 implied that it was not significantly relative to the pure error. There was a 16.09% chance that such a large lack-of-fit F-value could occur due to noise. The ANOVA test for the COD reduction efficiency (Table 5) showed that the model's F-value

Table 4
ANOVA for response function Y_1 (viscosity reduction efficiency) and variables selected to fit a model

Source	Sum of squares	df	Mean square	F-value	p-value prob. > F	Remark[a]
Model	2,171.06	9	241.23	27.70	0.0010	S
X_1	28.13	1	28.13	3.23	0.1322	NS
X_2	0.61	1	0.61	0.069	0.8026	NS
X_3	911.65	1	911.65	104.69	0.0002	S
X_1X_2	20.25	1	20.25	2.33	0.1878	NS
X_1X_3	1.96	1	1.96	0.23	0.6552	NS
X_2X_3	13.69	1	13.69	1.57	0.2653	NS
X_1^2	837.24	1	837.24	96.14	0.0002	S
X_2^2	273.61	1	273.61	31.42	0.0025	S
X_3^2	239.77	1	239.77	27.53	0.0033	S
Residual	43.54	5	8.71			
Lack-of-fit	38.73	3	12.91	5.37	0.1609	NS
Pure error	4.81	2	2.40			
Cor total	2,214.60	14				

[a]S: significant at $p < 0.05$; NS: not significant.

Table 5
ANOVA test for response function Y_2 (COD reduction efficiency) and variables selected to fit a model

Source	Sum of squares	df	Mean square	F-value	p-value prob. > F	Remark[a]
Model	1,359.99	9	151.11	45.22	0.0003	S
X_1	52.53	1	52.53	15.72	0.0107	S
X_2	13.00	1	13.00	3.89	0.1056	NS
X_3	712.53	1	712.53	213.22	<0.0001	S
X_1X_2	22.56	1	22.56	6.75	0.0483	S
X_1X_3	0.81	1	0.81	0.24	0.6433	NS
X_2X_3	3.80	1	3.80	1.14	0.3349	NS
X_1^2	212.80	1	212.80	63.68	0.0005	S
X_2^2	116.48	1	116.48	34.86	0.0020	S
X_3^2	305.20	1	305.20	91.33	0.0002	S
Residual	16.71	5	3.34			
Lack-of-fit	6.50	3	2.17	0.42	0.7572	NS
Pure error	10.21	2	5.10			
Cor total	1,376.70	14				

[a]S: significant at $p < 0.05$; NS: not significant.

was 45.22, implying that the model was significant. The probability of a larger F-value due to the uncontrollable noise factors were observed to be less (0.03%). The p-values less than 0.05 indicated that the model terms X_1, X_3, X_1X_2, X_1^2, X_2^2, and X_3^2 were significant. The lack-of-fit F-value of 0.42 implied that the lack-of-fit was not significant relative to the pure error, which further confirmed the reliability of the models [30,36].

The suitability of the selected models for providing adequate estimations of real systems was also confirmed by plots, such as the normal probability plots of the studentized residuals and the predicted vs. actual value plots. Fig. 3(a) and (b) shows the normal probability plot for the studentized residuals of the viscosity reduction and COD reduction efficiency, respectively. It can be deduced from the plots that the data were evenly distributed.

These models were also tested using the determination coefficient (R^2). The closer the R^2 values are to 1, the stronger the models are and the better they predict viscosity reduction and COD reduction rate. The determination coefficients ($R^2 = 0.9781$ for viscosity reduction and $R^2 = 0.9806$ for COD reduction) showed that only 2.19% (viscosity reduction) and 1.94% (COD reduction) of the variability in the responses were not explained by the models. In addition, the values of the adjusted determination coefficients ($R^2_{adj} = 0.9449$ for viscosity reduction and $R^2_{adj} = 0.9660$ for COD reduction) were also very high, showing a high significance of the models. Moreover, the values of the predicted R^2 were also high, supporting the significance of the models. Thus, the predicted

R^2 of 0.9803 for viscosity reduction efficiency and 0.9879 for COD reduction efficiency were in reasonable agreement with the adjusted R^2 of 0.9449 for viscosity reduction efficiency and 0.9660 for COD reduction efficiency, respectively. These results illustrate that the data prediction ability of the response surface model was satisfactory (Fig. 4(a) and (b)).

3.3. Interactive effect of the process variables

Three-dimensional response surface plots (Fig. 5) of the models generated by the Design Expert 8.0 software were used to evaluate the interactive effect of the independent variables on the responses. In Fig. 5(a), a 3D-response surface plot was developed as a function of current density (X_1) and inter-electrode gap (X_2) at the operation time of 20 min. At 20 mA/cm², the viscosity reduction increased by 3.8% (from 65.3 to 69.1%) as the inter-electrode gap was increased from 2.0 to 6.0 cm; whereas at 60 mA/cm², the viscosity reduction decreased by 5.2% (from 69.2 to 64.0%) when the inter-electrode gap was increased from 2.0 to 6.0 cm. As illustrated by the gradient in the surface plot, the current density was dominant in the interactive effect of current density/inter-electrode gap on the viscosity reduction. The viscosity reduction efficiency firstly increased with current density increasing from 20 to 40 mA/cm² and then reached a plateau when current density was up to 40 mA/cm². Due to the higher current, the amount of metal oxidized increased, resulting in a greater amount of precipitate for the fast reduction of organic pollutants [25]. One of
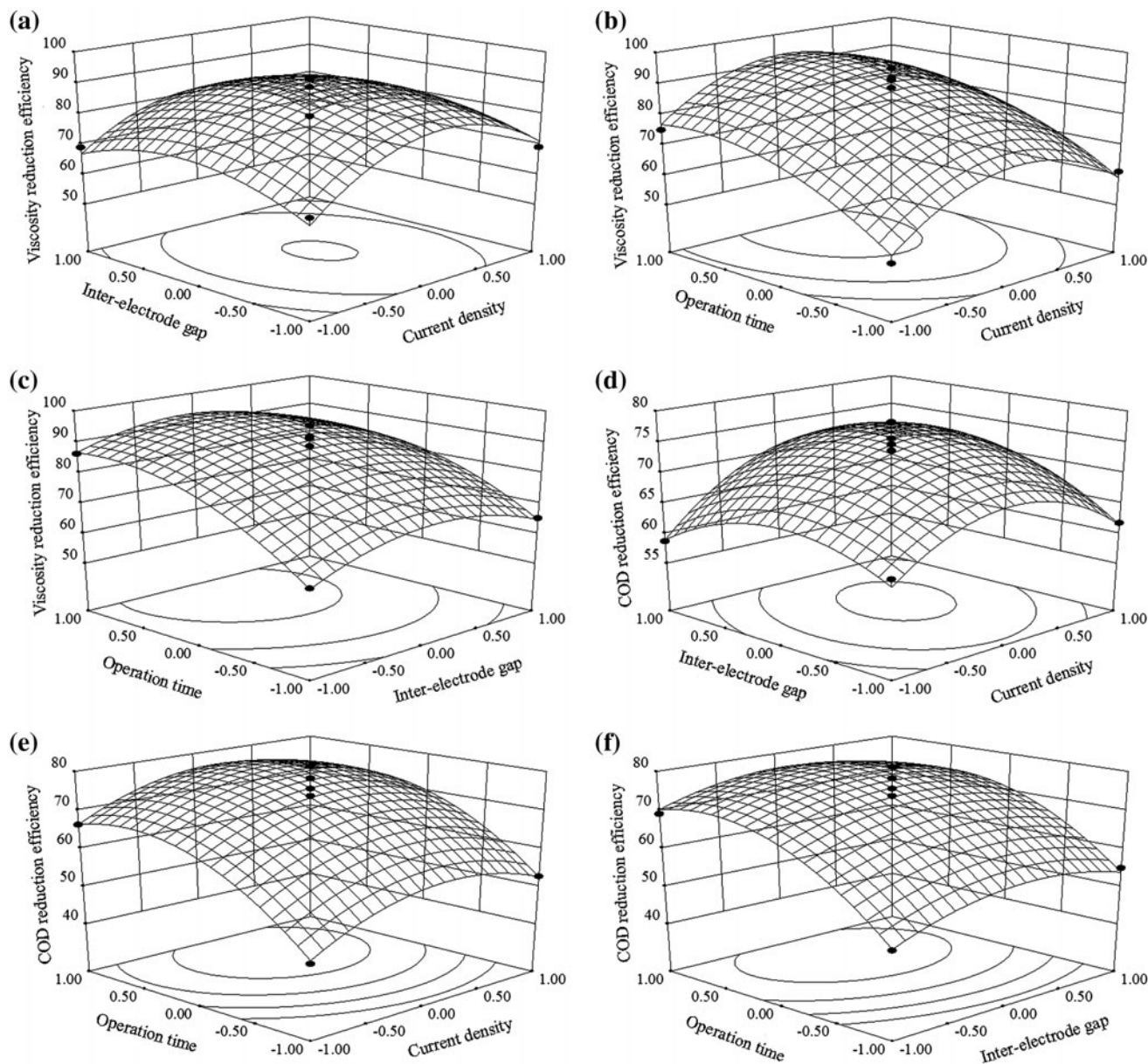
Fig. 5. Response surface plots of interactive effect among factors on (a–c) viscosity reduction (%) and (d and e) COD reduction efficiency (%).

the problems caused using aluminum as an electrode material is the formation of a passive oxide film, which inhibits the electrocoagulation process. This is the potential reason for such a slight decline in the reduction efficiency when the current density exceeded the optimum condition. Zhu et al. reported similar phenomenon for the removal of antimony from antimony mine flotation wastewater by EC process [28].

Fig. 5(b) describes the interaction between the current density and operation time with an inter-electrode gap of 4.0 cm. Increasing the operation time led to an increase in viscosity reduction in the current density investigated, and this effect was more significant at the operation time of 25 min. At 20 mA/cm^2, the viscosity reduction increased by 23.4% (from 51.7 to 75.1%) as the operation time was increased from 15 to 25 min; whereas at 60 mA/cm^2, the viscosity

reduction increased by 20.6% (from 61.2 to 81.8%) when the operation time increased from 15 to 25 min. Previous studies [26,28,37] have shown that the solubility of Al(OH)$_3$ is less at pH 6–8, whereas at pH 4–8, the Al^{3+} and OH$^-$ ions generated by electrodes react to form insoluble amorphous Al(OH)$_{3(S)}$ through a range of complex reactions. The plots show that an increase in operation time resulted in an increase in the viscosity reduction efficiency due to prolonged interaction between the Al(OH)$_3$ and polymer molecules.

Fig. 5(c) shows the interactive effect between the inter-electrode gap and operation time on the viscosity reduction efficiency at a steady state with a current density of 40 mA/cm^2. At 2.0 cm, the viscosity reduction reached 61.9 and 86.3% for operation times of 15 and 25 min, respectively; whereas at 6.0 cm, 65.2, and 82.2% of the viscosity reduction was obtained at operation times of 15 and 25 min, respectively. The rise in the viscosity reduction efficiency might be attributed to the fact that when the electrolysis time increased, the concentration of metal ions and hydroxide flocs increased.

Fig. 5(d) shows that COD reduction efficiency decreased by 3.6% (from 62.3 to 58.7%) and then increased by 5.9% (from 61.8 to 67.7%) when the current density was increased from 20 to 60 mA/cm^2 and the inter-electrode gap increased from 2.0 to 6.0 cm. At lower current density, as the distance between the electrodes increased, the resistance provided by the cell increased, and the electrical conductivity was proportional to the inter-electrode gap. According to Faraday's law, the amount of metal oxidized decreases with distance, which might explain the decline in the COD reduction efficiency while the electrode gap ranged from 2.0 to 6.0 cm [39,40]. The efficiency would be subsequently enhanced by a higher current density, which increases the rate of production of the coagulant.

Fig. 5(e) illustrates the interactive effect between current density and operation time at an inter-electrode gap of 4.0 cm. Current density and operation time were considered as the sensitive operating parameters in the electrocoagulation process. These two variables determine the coagulant production rate and total production of the coagulant. From the plot it was observed that at 15 min, the COD reduction increased by 6.9% (from 45.9 to 52.8%) as the current density increased from 20 to 60 mA/cm^2; whereas at 25 min, the COD reduction increased by 5.1% (from 66.4 to 71.5%) when the current density increased from 20 to 60 mA/cm^2. This is due to the increase in the quantity of aluminum released in the solution as a result of higher current density and longer reaction time, which enhance the formation of aluminum hydroxides and leads to higher COD reduction. Several studies have confirmed the individual/combined effect of current density and operation time on wastewater treatment efficiency. Attour et al. [26] noted that these parameters are linked, as pH changes in the process of electrocoagulation are due to the OH$^-$ production flux rate at the cathode. The pH increased with electrolysis time, resulting in an appreciable effect on the current density. Similar observations were also reported by other researchers [41].

Fig. 5(f) illustrates the individual/combined effects of inter-electrode gap and operation time when current density was at its zero level. It was obvious that the interactive effect of operation time and inter-electrode gap on the COD reduction exhibited the same tendency as on the viscosity reduction. The efficiency increased with increasing inter-electrode gap and operation time. There was a gradual increase in the COD reduction to the maximum with the increase in inter-electrode (from 2.0 to 4.0 cm) and operation time (from 15 to 20 min), and then a decrease with further distance and time enhancements (distance greater than 4.0 cm, time greater than 20 min).

3.4. Process optimization and model validation

To identify the optimum conditions for maximizing the reduction efficiency of viscosity and COD within the experimental ranges studied, the desirable point prediction function in the experimental design was applied. The predicted optimal results for viscosity and COD reduction were predicted to occur under the following conditions: a current density of 45.6 mA/cm^2, an inter-electrode gap of 3.2 cm, and an operation time of 22.8 min. The actual value of viscosity and COD reduction was 90.9 and 74.9%, respectively, which were in good agreement with the actual values from the regression models, with relatively small errors of 2.0 and 2.7%, respectively.

To confirm the predicted results, experiments were conducted using the optimum conditions that were given by the optimization software. Each experiment was repeated three times. Table 6 shows that the mean values for the viscosity and COD reduction were close to the predicted values.

3.5. Absorbance spectra of the samples

To assess the efficiency of the electrocoagulation treatment, the Gangxi 43# OPFPW (residual oil content: 47.2 mg/L, polymer content: 300 mg/L) and LPPFW were treated under the optimized conditions.

Table 6
Verification test of the fitting models

Test number	Operation parameters			Y_1 (%)			Y_2 (%)		
	X_1	X_2	X_3	Observed value	Predicted value	% Error	Observed vale	Predicted value	% Error
1	−0.7	−0.5	0.8	84.2	83.6	−1.0	71.2	71.5	0.4
2	−0.3	−0.6	−0.4	77.8	78.5	1.0	64.2	65.9	2.5
3	−0.3	−0.3	0.9	90.2	91.7	1.6	75.1	75.6	0.7
4	−0.5	−0.1	1.0	89.3	88.6	−1.0	72.7	73.5	1.1
5	0.2	0.4	−0.5	81.6	82.9	1.5	71.4	70.1	−1.9
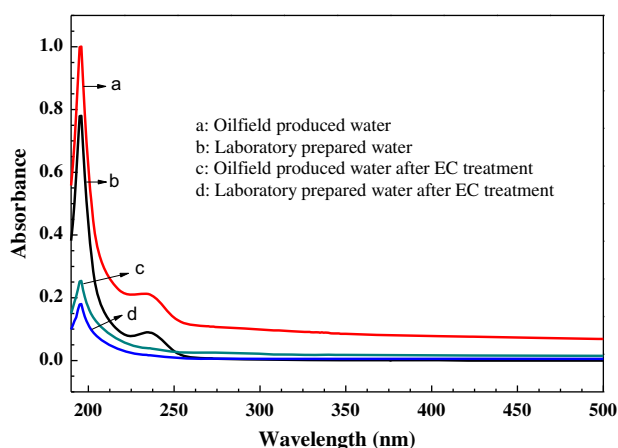
Fig. 6. Absorption spectra obtained from UV–vis analysis of the polymer solution samples before and after electrocoagulation treatment under the optimum conditions (a–d: diluted 10 times).

Fig. 6 shows the evolution of the UV–vis spectra of the polymer solution before and after the treatment. The absorption spectra of (a) and (b) represent the OPFPW and LPPFW samples, respectively. The curves of (c) and (d) show the spectra of these two water samples treated under the optimized conditions (i.e. a current density of 45.6 mA/cm², inter-electrode gap of 3.2 cm, and electrolysis time of 22.8 min). It is clear that the intensity of the characteristic band (195–196 nm) of the polymer solution samples was significantly reduced.

3.6. Calculation of zeta potential and operating costs

To calculate the aggregation efficiency, zeta potential (ζ, mV) measurement was applied in the OPFPW electrocoagulation process under the optimized conditions. At predetermined time intervals, solution samples were analyzed by nanozetasizer. There is a slight rise in absolute zeta potential (ranged from 40.33 to 41.35 mV) and remarkable increase in the average

particle size (ranged from 0 to 12.2 μm) with the reaction time. While pH was increasing, ambient conditions became favorable for aluminum hydroxide formation [42]. The acceleration in floc size was observed in the process, this was likely due to the agglomeration of micro-flocs. During this coagulation process, micro particles and charged organic matter were attached to the colloidal flocs by electrostatic force. As described in Fig. 7, the zeta potential values
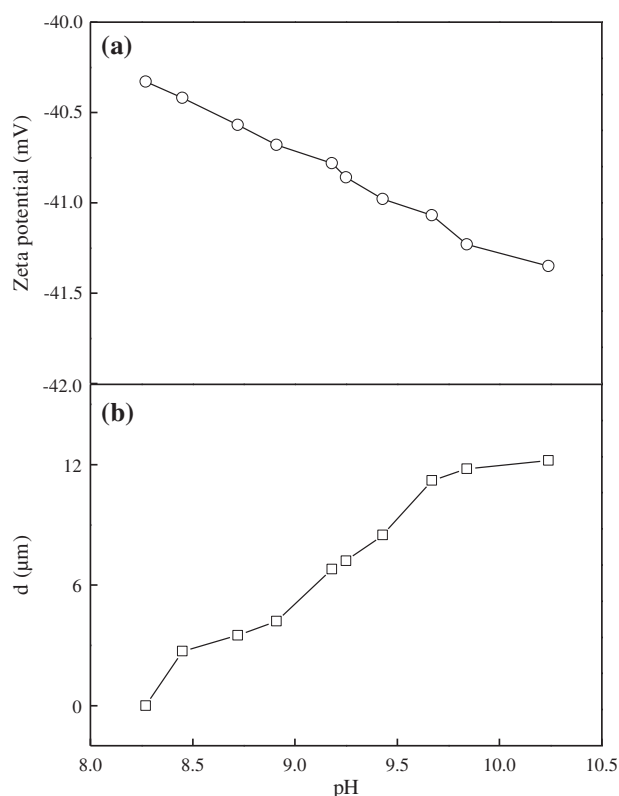
Fig. 7. Zeta potentials and diameters of freshly formed precipitates in the oilfield produced water treatment (from 0 min to the end) under the optimal conditions (1,000 mL of 47.2 mg/L oil content, and 300 mg/L polymer content of electrolysis solution, 45.6 mA/cm² current density, 3.2 cm inter-electrode gap, and 22.8 min operation time).

Table 7
Operational cost analysis for electrocoagulation (under the optimal conditions: current density of 45.6 mA/cm^2, inter-electrode gap of 3.2 cm, and operation time of 22.8 min)

Item	Operational parameter values	Cost ($/m^3)
Energy consumption	8.7 kW h/m^3	1.015
Electrode plate consumption	0.265 g/A h	0.433
Total		1.448

indicated a strong negative charge on the suspensions. The possible reason for this phenomenon is that ion adsorption. The surface dissociation has acted between the solid/aqueous phase. Similar observation was also reported by other investigators [42]. Under optimum condition, the energy and electrode consumptions were calculated to be 1.015 and 0.433 US $/m^3. From Table 7, the total consumption was found to be 1.448 US $/m^3.

4. Conclusions

In this study, second-order polynomial equations were built to describe the electrocoagulation process. The single variable X_3 was significant in terms of viscosity reduction, whereas the single effect of X_1 and X_3, the interactive effect of X_1X_2 significantly affected the COD reduction efficiency. The optimum conditions were found at a current density of 45.6 mA/cm^2, inter-electrode gap of 3.2 cm, and operation time of 22.8 min. Under such conditions, a 90.9% viscosity reduction and 74.9% COD reduction were achieved, which conformed to the predicted values of the model. The successful application of the RSM–BBD suggested that this is a new method for optimizing OPFPW treatment. Under the optimized conditions, there is a slight rise in absolute zeta potential and increase in the average particle size with the operation time. Future research on the optimization of the approach should be conducted on a large-scale that considers both energy consumption and electrode consumption.

Acknowledgments

References

[1] A. Maghzi, R. Kharrat, A. Mohebbi, M.H. Ghazanfari, The impact of silica nanoparticles on the performance of polymer solution in presence of salts in polymer flooding for heavy oil recovery, Fuel 123 (2014) 123–132.

[2] S.W. Giese, S.E. Powers, Using polymer solutions to enhance recovery of mobile coal tar and creosote DNAPLs, J. Contam. Hydrol. 58 (2002) 147–167.

[3] G.L. Jing, L.J. Xing, W.T. Du, C.J. Han, Development of a four-grade and four-segment electrodialysis setup for desalination of polymer-flooding produced water, Desalination 264 (2010) 214–219.

[4] J.L. Jing, X.Y. Wang, C.J. Han, The effect of oilfield polymer-flooding wastewater on anion-exchange membrane performance, Desalination 220 (2008) 386–393.

[5] B. Gao, Y. Jia, Y. Zhang, Q. Li, Q. Yue, Performance of dithiocarbamate-type flocculant in treating simulated polymer flooding produced water, J. Environ. Sci. 23 (2011) 37–43.

[6] D.K. Ramsden, K. McKay, Degradation of polyacrylamide in aqueous solution induced by chemically generated hydroxyl radicals: Part I—Fenton's reagent, Polym. Degrad. Stab. 14 (1986) 217–229.

[7] J.W. Qian, X.J. Xiang, W.Y. Yang, M. Wang, B.Q. Zheng, Flocculation performance of different polyacrylamide and the relation between optimal dose and critical concentration, Eur. Polym. J. 40 (2004) 1699–1704.

[8] V.F. Kurenkov, H.G. Hartan, F.I. Lobanov, Degradation of polyacrylamide and its derivatives in aqueous solutions, Russ. J. Appl. Chem. 75 (2002) 1039–1050.

[9] B. Wang, Y. Chen, S. Liu, H. Wu, H. Song, Photocatalytical visbreaking of wastewater produced from polymer flooding in oilfields, Colloids Surf., A 287 (2006) 170–174.

[10] C. Wu, A. Li, L. Li, L. Zhang, H. Wang, X. Qi, Q. Zhang, Treatment of oily water by a poly(vinyl alcohol) ultrafiltration membrane, Desalination 225 (2008) 312–321.

[11] S. Deng, R. Bai, J.P. Chen, Z. Jiang, G. Yu, F. Zhou, Z. Chen, Produced water from polymer flooding process in crude oil extraction: Characterization and treatment by a novel crossflow oil–water separator, Sep. Purif. Technol. 29 (2002) 207–216.

[12] M. Bao, Q. Chen, Y. Li, G. Jiang, Biodegradation of partially hydrolyzed polyacrylamide by bacteria isolated from production water after polymer flooding in an oil field, J. Hazard. Mater. 184 (2010) 105–110.

[13] Q. Wen, Z. Chen, Y. Zhao, H. Zhang, Y. Feng, Biodegradation of polyacrylamide by bacteria isolated from activated sludge and oil-contaminated soil, J. Hazard. Mater. 175 (2010) 955–959.

[14] X. Dai, F. Luo, J. Yi, Q. He, B. Dong, Biodegradation of polyacrylamide by anaerobic digestion under mesophilic condition and its performance in actual dewatered sludge system, Bioresour. Technol. 153 (2014) 55–61.

[15] M. Lu, X. Wei, Treatment of oilfield wastewater containing polymer by the batch activated sludge reactor combined with a zerovalent iron/EDTA/air system, Bioresour. Technol. 102 (2011) 2555–2562.

[16] X. Qiao, Z. Zhang, J. Yu, X. Ye, Performance characteristics of a hybrid membrane pilot-scale plant for oilfield-produced wastewater, Desalination 225 (2008) 113–122.

[17] X. Wang, Z. Wang, Y. Zhou, X. Xi, W. Li, L. Yang, X. Wang, Study of the contribution of the main pollutants in the oilfield polymer-flooding wastewater to the critical flux, Desalination 273 (2011) 375–385.

[18] Y. Zhang, B. Gao, L. Lu, Q. Yue, Q. Wang, Y. Jia, Treatment of produced water from polymer flooding in oil production by the combined method of hydrolysis acidification-dynamic membrane bioreactor–coagulation process, J. Petrol. Sci. Eng. 74 (2010) 14–19.

[19] J. Llanos, S. Cotillas, P. Cañizares, M.A. Rodrigo, Effect of bipolar electrode material on the reclamation of urban wastewater by an integrated electrodisinfection/electrocoagulation process, Water Res. 53 (2014) 329–338.

[20] M. Taheri, M.R. Alavi Moghaddam, M. Arami, Techno-economical optimization of Reactive Blue 19 removal by combined electrocoagulation/coagulation process through MOPSO using RSM and ANFIS models, J. Environ. Manage. 128 (2013) 798–806.

[21] A. Shafaei, E. Pajootan, M. Nikazar, M. Arami, Removal of Co(II) from aqueous solution by electrocoagulation process using aluminum electrodes, Desalination 279 (2011) 121–126.

[22] Ö. Hanay, H. Hasar, Effect of anions on removing Cu^{2+}, Mn^{2+} and Zn^{2+} in electrocoagulation process using aluminum electrodes, J. Hazard. Mater. 189 (2011) 572–576.

[23] E. Gengec, M. Kobya, E. Demirbas, A. Akyol, K. Oktor, Optimization of baker's yeast wastewater using response surface methodology by electrocoagulation, Desalination 286 (2012) 200–209.

[24] M. Tir, N. Moulai-Mostefa, Optimization of oil removal from oily wastewater by electrocoagulation using response surface method, J. Hazard. Mater. 158 (2008) 107–115.

[25] P. Maha Lakshmi, P. Sivashanmugam, Treatment of oil tanning effluent by electrocoagulation: Influence of ultrasound and hybrid electrode on COD removal, Sep. Purif. Technol. 116 (2013) 378–384.

[26] A. Attour, M. Touati, M. Tlili, M. Ben Amor, F. Lapicque, J.P. Leclerc, Influence of operating parameters on phosphate removal from water by electrocoagulation using aluminum electrodes, Sep. Purif. Technol. 123 (2014) 124–129.

[27] Y.O. Fouad, Separation of cottonseed oil from oil–water emulsions using electrocoagulation technique, Alexandria Eng. J. 53 (2014) 199–204.

[28] J. Zhu, F. Wu, X. Pan, J. Guo, D. Wen, Removal of antimony from antimony mine flotation wastewater by electrocoagulation with aluminum electrodes, J. Environ. Sci. 23 (2011) 1066–1071.

[29] H. Zhang, X. Ran, X. Wu, D. Zhang, Evaluation of electro-oxidation of biologically treated landfill leachate using response surface methodology, J. Hazard. Mater. 188 (2011) 261–268.

[30] A. Mujtaba, M. Ali, K. Kohli, Statistical optimization and characterization of pH-independent extended-release drug delivery of cefpodoxime proxetil using Box-Behnken design, Chem. Eng. Res. Des. 92 (2014) 156–165.

[31] D. Das, R. Vimala, N. Das, Biosorption of Zn(II) onto *Pleurotus platypus*: 5-Level Box–Behnken design, equilibrium, kinetic and regeneration studies, Ecol. Eng. 64 (2014) 136–141.

[32] M.J. Chaichi, S.N. Azizi, O. Alijanpour, M. Heidarpour, M. Qandalee, Application of Box-Behnken design in the optimization of new peroxyoxalate–H_2O_2 chemiluminescence system using furan derivatives as blue activators, J. Lumin. 138 (2013) 65–71.

[33] J. Prakash Maran, S. Manikandan, V. Mekala, Modeling and optimization of betalain extraction from *Opuntia ficus*-indica using Box–Behnken design with desirability function, Ind. Crop. Prod. 49 (2013) 304–311.

[34] D. Ghosh, C.R. Medhi, M.K. Purkait, Treatment of fluoride containing drinking water by electrocoagulation using monopolar and bipolar electrode connections, Chemosphere 73 (2008) 1393–1400.

[35] J. Prakash Maran, S. Manikandan, K. Thirugnanasambandham, C. Vigna Nivetha, R. Dinesh, Box–Behnken design based statistical modeling for ultrasound-assisted extraction of corn silk polysaccharide, Carbohydr. Polym. 92 (2013) 604–611.

[36] Y.D. Chen, W.Q. Chen, B. Huang, M.J. Huang, Process optimization of $K_2C_2O_4$-activated carbon from kenaf core using Box–Behnken design, Chem. Eng. Res. Des. 91 (2013) 1783–1789.

[37] M.H. Isa, E.H. Ezechi, Z. Ahmed, S.F. Magram, S.R.M. Kutty, Boron removal by electrocoagulation and recovery, Water Res. 51 (2014) 113–123.

[38] C. Thakur, V.C. Srivastava, I.D. Mall, Electrochemical treatment of a distillery wastewater: Parametric and residue disposal study, Chem. Eng. J. 148 (2009) 496–505.

[39] I. Heidmann, W. Calmano, Removal of Cr(VI) from model wastewaters by electrocoagulation with Fe electrodes, Sep. Purif. Technol. 61 (2008) 15–21.

[40] S. Zodi, O. Potier, F. Lapicque, J.P. Leclerc, Treatment of the industrial wastewaters by electrocoagulation: Optimization of coupled electrochemical and sedimentation processes, Desalination 261 (2010) 186–190.

[41] F. Ulu, S. Barışçı, M. Kobya, H. Särkkä, M. Sillanpää, Removal of humic substances by electrocoagulation (EC) process and characterization of floc size growth mechanism under optimum conditions, Sep. Purif. Technol. 133 (2014) 246–253.

[42] E. Ofir, Y. Oren, A. Adin, Electroflocculation: The effect of zeta-potential on particle size, Desalination 204 (2007) 33–38.